Interface between a Polysulfone and Polyamide As Studied by Combined Neutron Reflectivity and Small-Angle Neutron Scattering Techniques

ARTICLE *in* MACROMOLECULES · OCTOBER 2000

Impact Factor: 5.8 · DOI: 10.1021/ma000661g · Source: OAI

10 AUTHORS, INCLUDING:

Hirokazu Hasegawa
Kyoto University
163 PUBLICATIONS **4,916** CITATIONS

SEE PROFILE

Mikihito Takenaka
Kyoto University
145 PUBLICATIONS **1,811** CITATIONS

SEE PROFILE

Alan R Esker
Virginia Polytechnic Institute and State Univ…
103 PUBLICATIONS **1,071** CITATIONS

SEE PROFILE

Interface between a Polysulfone and Polyamide As Studied by Combined Neutron Reflectivity and Small-Angle Neutron Scattering Techniques

M. Hayashi,[†] T. Hashimoto,*[,†] H. Hasegawa,[†] M. Takenaka,[†] H. Grüll,[‡,§] A. R. Esker,[‡,%] M. Weber,[⊥] S. K. Satija,[§] C. C. Han,[‡] and M. Nagao[#]

Department of Polymer Chemistry, Graduate School of Engineering, Kyoto University, Kyoto 606-8501, Japan; Polymers Division and NIST Center for Neutron Research, National Institute of Standards and Technology (NIST), Gaithersburg, Maryland 20899; BASF Aktiengesellschaft, Polymer Research Laboratory, Engineering Plastics, D-67056 Ludwigshafen, Germany; and Neutron Scattering Facility, Institute for Solid State Physics, The University of Tokyo, Tokai, Naka-gun, Ibaraki-ken, Japan

Received April 14, 2000; Revised Manuscript Received August 17, 2000

ABSTRACT: Interfaces between the two phases formed in immiscible polymer pairs were studied by means of neutron reflectivity (NR) combined with small-angle neutron scattering (SANS). The interfacial widths evaluated by the two methods were compared for two systems: a nonreactive system composed of polyamide (PA) and polysulfone (PSU) and a reactive system composed of PA and PSU with a phthalic anhydride reactive end group (PSU-R) in which PSU-*b*-PA block copolymers can be formed at the interface. SANS measurements were made on bulk mixtures, and the NR measurements were performed on thin film bilayer stacks of PA and PSU or PSU-R. The intrinsic interfacial widths, $W_{I,diffuse}$, obtained from the two methods were compared for the samples that underwent similar annealing protocols and were quenched below the glass transition temperatures T_g's to room temperature. A consistent result for $W_{I,diffuse}$ can be obtained for the two methods only after taking into account the following important factors: (i) the SANS intensity should be corrected for the frozen density heterogeneities within each phase as well as the frozen thermal composition fluctuations; (ii) the contribution of capillary wave fluctuations to a net (or observed) interfacial width, $W_{I,obs}$, is more significant for NR than SANS. Without the former correction, the SANS profiles at high scattering vector, q, showed asymptotic behavior of q^{-n} ($n < 4$), giving an erroneous conclusion on $W_{I,obs}$. The $W_{I,obs}$ values obtained for the reactive system were found to be larger than those for the nonreactive system for both methods, reflecting block copolymer formation at the interfaces. The interfacial area density, Σ, for the bulk mixture of the reactive system rapidly decreased with time and reached a constant value within ca. 2 min after annealing above the T_g's, while Σ for the nonreactive system kept decreasing with time. This elucidates that the growth of the phase-separating domains in the reactive system was pinned by the formation of block copolymers at the interfaces during early annealing times.

I. Introduction

Incompatible blends usually suffer from a lack of adhesion along the phase-separated domain boundaries which provides a reason for mechanical failures. Their behaviors, morphology, and the interfacial properties have been the subjects of intensive studies over the past decades, especially from the viewpoint of industrial applications. As polymer blends in practical use are usually immiscible, understanding those matters described above is necessary for controlling phase-separated structures on a mesoscopic scale as well as to improve mechanical and rheological properties for the desired applications. The overall physical properties of immiscible polymer blends critically depend on coupled parameters such as the interfacial tension, γ, adhesion between the two phases and the size of the phase-separated structures. For example, interfacial mixing of two components,[1] which depends on γ, influences the interfacial adhesion of the two phases, which ultimately controls the physical and the mechanical properties of the blend.[2−5]

One way to achieve improved adhesion in incompatible systems is to add reactive polymer components which can form a graft or block copolymer through an interfacial reaction.[5,6] Fracture toughness of the reactive system was certainly shown to be higher than that of the nonreactive counterpart (see for example ref 7). Although reactive blending is widely used in industrial processes, it is still a matter of ongoing research to characterize the underlying principles. One point of interest is the open question whether sufficient diblock can be formed through an interfacial reaction to significantly reduce the interfacial tension of the system and significantly increase the interfacial width between polymer phases.[8−11] Our primary objective in this work is not to explore mechanical performance of the interface but rather to explore nature of the interface created by reactive blending and to compare this result with those obtained for the nonreactive system. The results will clearly elucidate how the domain morphology is influenced by the reactivity.

[†] Kyoto University.
[‡] Polymers Division, NIST.
[§] NIST Center for Neutron Research, NIST.
[⊥] BASF Aktiengesellschaft.
[#] The University of Tokyo.
[$] Present address: Ben-Gurion University of the Negev, Department of Chemical Engineering, PO Box 653, Beer-Sheva 84105, Israel.
[%] Present address: Virginia Tech, Department of Chemistry, Blacksburg, VA 24061-0212.
* To whom correspondence should be addressed.

10.1021/ma000661g CCC: $19.00
Published on Web 10/14/2000

The composition profile of one component (component A in a binary blend of A and B) across the interface between two immiscible polymers, $\phi_A(z)$, is given by[12]

$$\phi_A(z) = {}^1/_2[1 + \tanh(z/W_{I,diffuse})] \quad (1)$$

where z is the coordinate normal to the interface and $W_{I,diffuse}$ is the intrinsic interfacial width. $W_{I,diffuse}$ is given in terms of the statistical segment length l and the Flory−Huggins interaction parameter χ[13] as

$$W_{I,diffuse} = 2l/(6\chi)^{1/2} \quad (2)$$

The interfacial widths for well-characterized immiscible polymer pairs of polystyrene (PS) and poly(methyl methacrylate) (PMMA) have been evaluated by means of neutron reflectivity (NR).[14−16] The observed interfacial width values, $W_{I,obs}$, were found to be significantly larger than those predicted by analytical theories,[12,17,18] revealing the importance of capillary wave contributions to the observed value. Nonetheless, multiple studies on thin films reveal that finite size effects can significantly alter the magnitude of capillary waves.[19] Previously reported results on the interfacial width for the reactive polymer system of this study[20] were obtained by NR in thin bilayer films. In bulk systems, scattering techniques such as SANS or SAXS can be employed to study the interfacial properties of polymer blends.[21] Here the $W_{I,obs}$'s measured by SANS or SAXS are also affected in general by the capillary wave fluctuations. However, the lateral dimension of the interface, which is much larger in bilayer films than for phase-separated bulk mixtures, is expected to significantly alter the contribution of capillary waves to the total observed interfacial width. Surprisingly, no systematic experiments comparing the interfacial widths obtained by both scattering and reflectivity exist to the best of our knowledge for the same polymer system.

In this study, bulk interfacial widths between immiscible polymers of A and B obtained by small-angle neutron scattering (SANS) are compared to the interfacial width observed in thin bilayer films using neutron reflectivity (NR). Hereafter, the systems studied are designated as substrate//A//B//air and substrate//A*//B// air for the bilayer system and A/B for the bulk mixture, where "//" and "/" designate a macroscopic interface between two layers and the conventional sign for a mixture, respectively. A* is A having a functional end group allowing a reaction with the end group of B to form a block copolymer A-*b*-B in an interfacial reaction. As described in our previous report,[20] this polymer pair A and B has a segregation power large enough so that A-*b*-B copolymers formed stay localized at the interface between the A- and B-rich phases. The formed copolymers lower the interfacial tension γ and hence increase the interfacial width $W_{I,diffuse}$. Advantages to the use of thin bilayer films of immiscible polymer pairs are as follows: (i) one can get a well-defined macroscopic interface between A and B, and (ii) one can analyze changes in composition profiles of A or B across the interface with a high accuracy by using specular NR before and after annealing. On the other hand, SANS allows an analysis of interfacial structures in bulk blends without the extensive sample preparation procedures required for NR. Thus, the two methods can provide complementary information depending upon experimental situations or purposes. From this viewpoint it is worthwhile to compare the results obtained by the two methods on common polymer systems.

Table 1. Characteristics of Polymers Used in This Study

			end group (%)			
polymer	N_w	N_w/N_n	PhAh	OH	Cl	T_g (°C)
dPSU[a]	58	3.51		3	97	176
dPSU-R[b]	80	6.27	50	35	15	174
PA[c]	3.3×10^4 [d]	3.90				113

[a] Deuterated polysulfone. [b] Deuterated polysulfone with phthalic anhydride group. [c] Polyamide, Grilamide, EMS, Switzerland. [d] Since an average degree of polymerization is not well defined, we indicated weight-average molecular weight here obtained from GPC (using HFIP as the solvent).

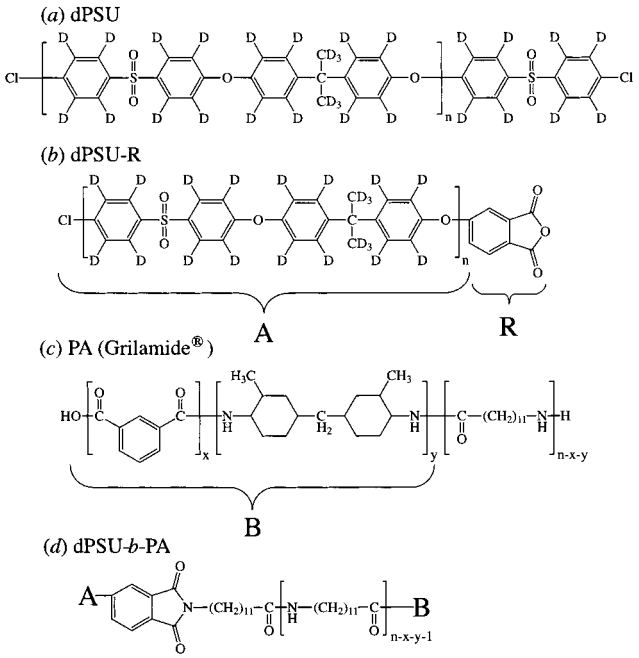

Figure 1. Chemical structures of (a) dPSU, (b) dPSU-R, (c) PA, and (d) dPSU-*b*-PA. Unfortunately *x*, *y*, and *n* are not well defined for the PA used in this work. This PA is not crystallizable from melts.

In general, NR provides information on interfacial widths between polymer layers with a depth resolution on the order of 0.2−0.8 nm through a dynamical theory of scattering[22] depending on the experimental conditions such as wave vector, q, range, film thickness, instrument setting, and so on. In contrast, the SANS interfacial width arises from the analysis of the SANS data at the large q tails through a kinematical theory of scattering,[23] i.e., an analysis concerning deviation of the asymptotic behavior of the SANS profile from Porod's law.[24]

II. Experimental Section

II.1. Polymers Used in the Present Study. All the polymer samples used in this study, deuterated polysulfone (dPSU), deuterated polysulfone with a phthalic anhydride end group (dPSU-R with R designating the phthalic anhydride end group), and a commercial aromatic polyamide, Grilamide (PA), were supplied and characterized by BASF Aktiengesellschaft, Ludwigshafen, Germany, and their characteristics are summarized in Table 1. The chemical structures of dPSU, dPSU-R, and PA are shown in Figure 1. Since an average degree of polymerization of PA as shown in Figure 1 is not well defined, the weight-average molecular weight for PA is given in Table 1. It should be noted that PA is totally amorphous. The DSC

Table 2. Specimens and Experimental Conditions

specimens	experiments	experimental conditions[a]
dPSU/PA	SANS (50/50 mixture by wt %)	annealed at 240 °C for 0−180 min
	NR (bilayer)	annealed at 210 °C for 0−755 min and 240 °C for 60 min
dPSU-R/PA	SANS (50/50 mixture by wt %)	annealed at 240 °C for 0−180 min
	NR (bilayer)	annealed at 210 °C for 0−755 min and 240 °C for 60 min

[a] All measurements were performed at room temperature.

thermogram of PA measured during heating after first quenching from a high enough temperature (∼250 °C) to room temperature did not show any features suggesting the melting of PA. Here, the T_g's of dPSU, dPSU-R, and PA are 176, 174, and 113 °C, respectively.[20] The R end group of dPSU-R can react with the terminal amino group of PA to form block copolymer chains dPSU-*b*-PA.

II.2. Preparation of Samples for SANS and NR Experiments. The experimental systems, methods employed, and respective preparation conditions, such as annealing temperature and time, are summarized in Table 2. The samples for the SANS experiments were prepared as follows. The dPSU or dPSU-R and the PA were separately dissolved in 1,1,1,3,3,3-hexafluoro-2-propanol (HFIP)/chlorobenzene (2/1 by volume) to obtain homogeneous solutions containing 5 wt % polymer. Syringe filters with 0.5 μm pores were used to separately filter each solution. The filtered solutions were mixed together in such a way that mixtures of 50 wt % dPSU or dPSU-R and PA were prepared and subsequently precipitated first in hexane and then several times in ethanol. The precipitated polymer mixtures were dried at 80 °C for 1 day under vacuum. The dried mixtures were melt-pressed at 180 °C for a few minutes under ca. 4 MPa between iron plates to form disks with thicknesses of 0.5 mm (dPSU-R/PA) or 1 mm (dPSU/PA) and diameters of 15 mm using a copper spacer ring. Subsequently, the disks were cooled slowly in air to room temperature. These samples are denoted hereafter as "as-melt-pressed" specimens.

Films for the NR measurements listed in Table 2 were prepared by spin-casting dPSU and dPSU-R from the 2 wt % chlorobenzene solutions onto silicon (Si) wafers (5 mm in thickness and 75 mm in diameter, purchased from Polishing Corporation of America, Santa Clara, CA). Prior to spin-coating, the Si wafers were treated by ozone plasma for 5 min to remove the surface organics. Subsequently, the wafers were cleaned by boiling in a bath containing 30% NH_4OH/30% H_2O_2/H_2O (1/1/4 by volume) for 1.5 h and then in a bath containing 70% concentrated H_2SO_4/30% H_2O_2 (7/3 by volume) also for 1.5 h. The silicon oxide layer on the Si surface was etched off by using a buffered 3% HF aqueous solution for 3 min, and the etched Si surface was stabilized by immersing in 40% NH_4F aqueous solution for 5 min.

To prepare the bilayer samples, a thick film of PA (∼2.0 μm) was spun-cast from 1 wt % solution in HFIP onto the hydrophilic surface of another Si wafer. By immersing the wafer into distilled water, the PA layer was floated off onto the water surface and was then picked up on the Si wafer spin-coated with dPSU or dPSU-R (ca. 60 nm thick) prepared in advance. Finally, the complete specimens were dried at 70 °C for 1 day under vacuum.

II.3. SANS and NR Experiments Performed in the Present Study. SANS experiments were performed on the SANS-U instrument at the JRR-3M research reactor at the Japan Atomic Energy Research Institute (JAERI), Tokai, Ibaragi, Japan. The prepared specimens were sandwiched between two copper windows of 0.1 mm thickness, annealed at the target temperature of 240 °C for a set period of time, and subsequently quenched to room temperature. The SANS measurements were performed at room temperature, and the scattered intensity was obtained as a function of q_S, which is defined by

$$q_S = (4\pi/\lambda_{SANS}) \sin(\theta_S/2) \quad (3)$$

where θ_S is the scattering angle of the neutrons, and λ_{SANS} is the wavelength of the incident neutron beam (7 Å) for SANS. The experimental and data reduction procedures detailed elsewhere were followed.[25] The acquired SANS intensity data were corrected for empty cell contributions and were finally converted to an absolute intensity scale using Lupolen as the secondary standard.

NR measurements were performed on the NG7 reflectometer at the NIST Center for Neutron Research (NCNR), National Institute of Standards and Technology, Gaithersburg, MD. The bilayer samples described in section II.2 were annealed for a set period of time at 210 °C, a temperature above the glass transition temperature of both components. Subsequently, the samples were quenched to room temperature for NR measurements. The Si wafers were placed with the bottom surface up, i.e., the sample on the polished Si surface facing down on the horizontal sample stage of NG7 to avoid the absorption of the incident neutron beam by the thick PA layer. Thus, all measurements were taken with the incident neutron beam coming in from the Si side, and the specularly reflected neutrons were captured with a pencil detector as a function of the magnitude of the scattering vector q_R, which is defined by

$$q_R = (4\pi/\lambda_{NR}) \sin(\theta_R) \quad (4)$$

where θ_R is the incident angle of the incident beam and reflection angle of the reflected beam to the sample surface, and λ_{NR} is the wavelength of the incident neutron beam used for NR (4.75 Å).

Both NR and SANS measurements were performed to elucidate the interfacial characteristics as a function of the annealing time for the PSU and PA blends. Hereafter the magnitude of the scattering vector will be designated simply as q for both SANS and NR results since q_S and q_R are essentially the same.

III. Results

III.1. SANS Characterization of the Bulk Mixtures. The SANS profiles for the nonreactive dPSU/PA system are plotted in Figure 2a. A significant change in the scattering profile occurs after the initial annealing step where the as-melt-pressed sample is heated for 2 min at 240 °C. Subsequent annealing leads to a slow decrease in the intensity at $q < 0.03$ Å^{-1}. Unlike the low q data, the intensity at $q > 0.06$ Å^{-1} stays almost constant for annealing times longer than or equal to 2 min.

The SANS profiles for the reactive end group labeled dPSU-R/PA system is shown in Figure 2b. The initial change of the scattering intensity with annealing is similar to dPSU/PA, where a pronounced change of the scattering profile was observed in the first 2 min of annealing. However, additional annealing does not produce any observable change in the SANS profiles contrary to the dPSU/PA system, implying a pinning of the structure evolution.

For all annealing times of the as-melt-pressed samples for $t > 2$ min, the scattering intensity $S(q)$ for both systems dPSU/PA and dPSU-R/PA shows a power law dependence over the q range of 0.007 Å$^{-1} < q < 0.02$ Å^{-1} according to Porod's law with $S(q) \sim q^{-n}$, $n \cong 4$. This power law behavior suggests the scattering in this q region arises from a sharp interface between the two coexisting phases. For both systems, a deviation of $S(q)$ from this power law is observed in the region of $q > 0.02$ Å^{-1}.

As for the as-melt-pressed sample it should be noted that the absolute intensity for dPSU/PA is higher than

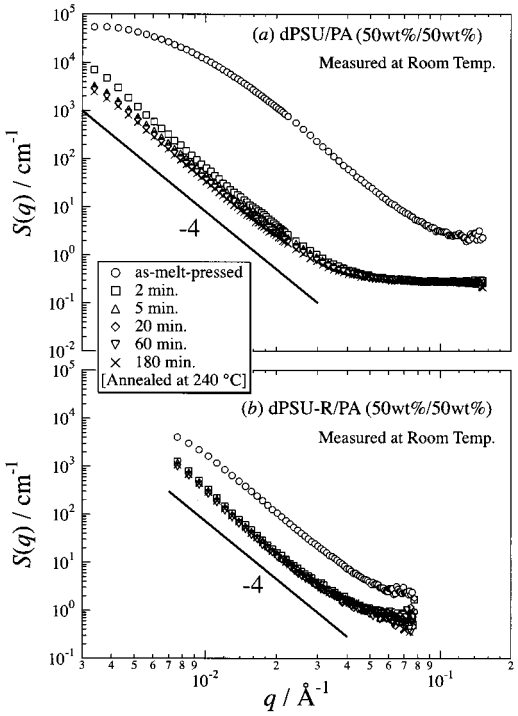

Figure 2. Change in the SANS profiles with annealing time for (a) dPSU/PA (50 wt %/50 wt %) and (b) dPSU-R/PA (50 wt %/50 wt %). These data were not corrected for intraphase density fluctuations.

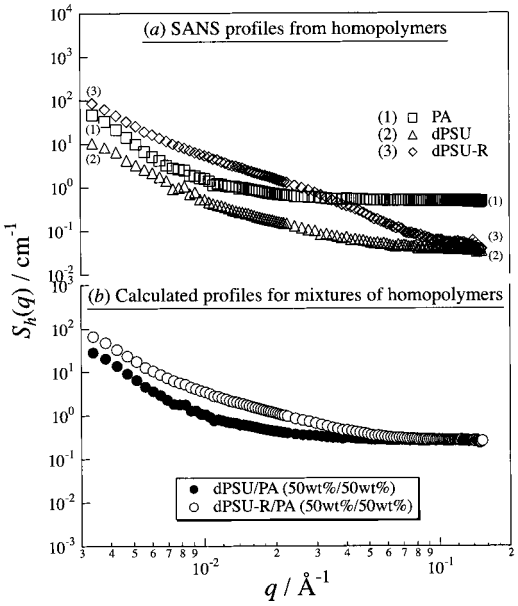

Figure 3. (a) SANS profiles measured for the homopolymers, dPSU, dPSU-R, and PA, and (b) the calculated scattering intensity distribution $S_h(q)$ which accounts for both scattering from the density heterogeneities within the phase-separated domains and incoherent scattering (see eq 9 in the text).

for dPSU-R/PA. On the other hand, the intensity level in the q range where q^{-4} is observed is now much higher for the reactive system than for the nonreactive system for annealing times greater than or equal to 2 min.

Figure 3a shows the SANS profiles for the neat polymers, i.e., (1) PA, (2) dPSU, and (3) dPSU-R. These data are important for the complete analysis presented in section IV.

III.2. NR Characterization of the Bilayer Samples. NR profiles obtained for the Si//dPSU//PA//air and Si//dPSU-R//PA//air systems are shown in Figure 4a,b corresponding to the as-prepared samples, samples annealed for 755 min at $T = 210$ °C, and samples annealed an additional 60 min at $T = 240$ °C. Results of NR experiments, taken with the same sample after annealing for 10, 30, 90, and 270 min at $T = 210$ °C, were reported elsewhere.[20] The NR data are fitted using a standard multilayer fitting routine for the scattering length density (SLD) profile as described elsewhere.[26] The solid lines in Figure 4 present the best fit of the experimental data assuming the model SLD depth profiles shown in the inset.

IV. Analysis and Discussion

IV.1. Correction of SANS Profiles for the Scattering Due to Heterogeneities in Each Phase-Separated Domain. IV.1.1. Scattering from Density Heterogeneities in Neat Homopolymers. Usually, the incoherent scattering is subtracted from raw SANS data in order to obtain SANS structure factors. In addition to this correction, the contribution of the density heterogeneities caused by vitrification[27] should be subtracted from the raw SANS data, since all the raw SANS data were obtained at room temperature, which is below T_g for all components. Figure 3a shows SANS profiles for each homopolymer at room temperature. In the absence of frozen density heterogeneities in each homopolymer sample, only incoherent scattering and thermal diffuse scattering would contribute to the total intensity $S(q)$. Furthermore, no remarkable q dependence should be observed in $S(q)$. Therefore, the strong q dependence of $S(q)$ is taken as evidence for the presence of frozen density heterogeneities at room temperature. In comparison, the contribution of the incoherent scattering in the SANS data of dPSU and dPSU-R is small. Thus, the incoherent intensity observed in the plateau region of $S(q)$, $q > 0.08$ Å^{-1}, is much lower for the deuterated polymers dPSU and dPSU-R than the incoherent intensity observed in the plateau region of $q > 0.03$ Å^{-1} for PA (Figure 3a). The SANS profile for dPSU-R shows a very broad peak or shoulder, at $q_m \cong 0.03$ Å^{-1} with a corresponding characteristic length Λ ($\equiv 2\pi/q_m$) = 200 Å.

Takeno et al. studied the miscibility of several polymer pairs prepared out of a given dPSU and two modified PSUs denoted by PSU-R1 and PSU-R2[28] by SANS. PSU-R1 and PSU-R2 are protonated PSU polymers with one phthalic anhydride end group and differ only in their molecular weight with a number-average degree of polymerization $N = 40$ (PSU-R1) and $N = 171$ (PSU-R2), respectively. Takeno et al. report that dPSU and PSU-R1 are immiscible whereas dPSU and PSU-R2 are miscible over the temperature range studied in their work, although dPSU and PSU-R are almost identical to each other in terms of chemical structure except for deuterium labeling and the phthalic anhydride end group. These results could be interpreted by assuming that there are strong repulsive interactions between dPSU or PSU units and the R end group. Because of its significantly higher molecular weight, PSU-R2 becomes miscible with dPSU due to a dilution effect of the repulsive interactions. In other words, if the PSU chains in PSU-R are longer than a certain length, dPSU and PSU-R are miscible. Furthermore, a strong repulsion between the dPSU unit and the R unit may cause an association of R end groups in the matrix composed of dPSU. This association causes the composi-

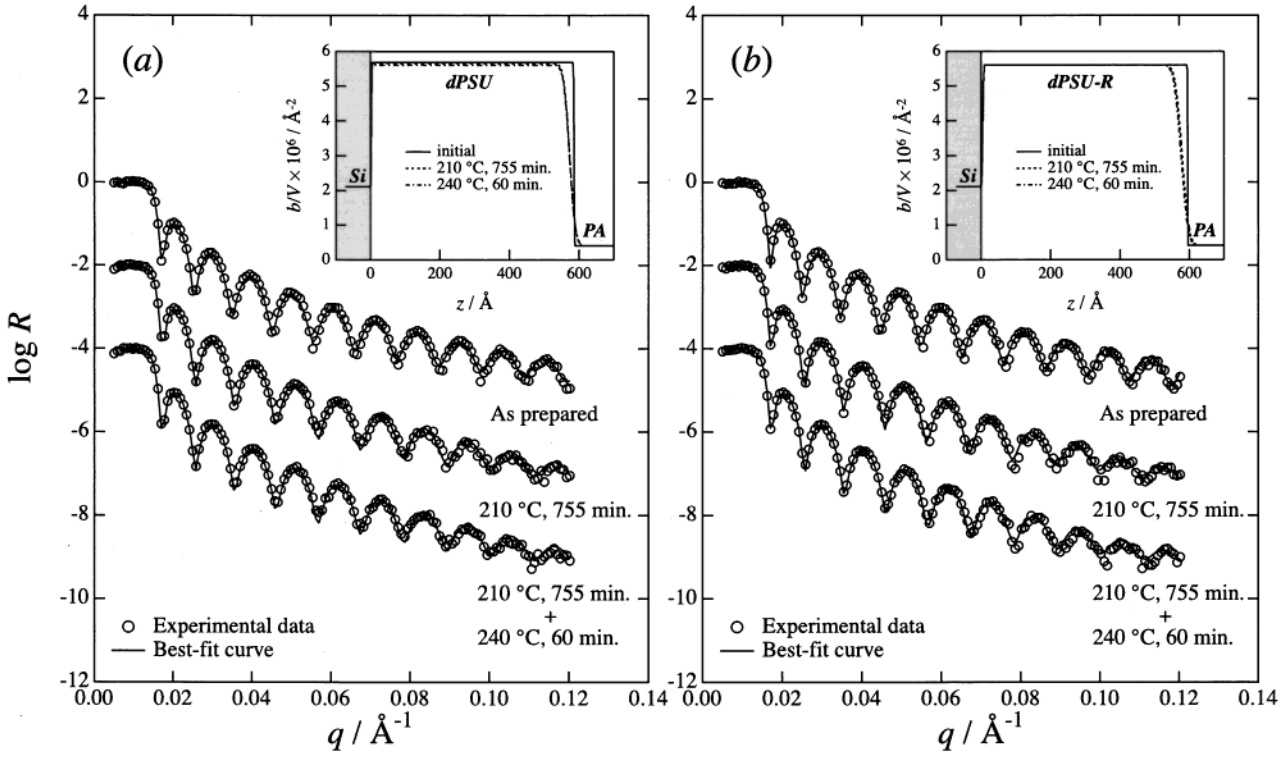

Figure 4. NR profiles (open circles) obtained from the as-prepared bilayers, the bilayers annealed at 210 °C for 755 min, and specimens annealed another 60 min at 240 °C for (a) Si//dPSU//PA//air and (b) Si//dPSU-R//PA//air. The best-fit curves for the respective NR profiles are given as solid lines, and the corresponding SLD profiles are shown in the insets of the respective figures.

tion fluctuations of the R units in the neat dPSU-R film, which accounts for the excess scattering from the dPSU-R homopolymer relative to the scattering from the dPSU homopolymer. It is conceivable that the association may further enhance the density heterogeneity upon a vitrification of dPSU-R.

IV.1.2. Correction of SANS Data for Density Heterogeneities within Phase-Separated Domains. The net scattering structure factor, $S_t(q)$, for the q range studied in the present work is given by

$$S_t(q) \equiv S_{\text{interf}}(q) + S_{\text{comp}}(q) + S_{\text{density}}(q) + S_{\text{incoh}} \quad (5)$$

where $S_{\text{interf}}(q)$ is the scattering from the interface between the phase-separated domains, which is detailed in section A-1 of the Appendix. Its q dependence is given by $S_{\text{interf}}(q) \sim q^{-n}$ with $n = 4$ for sharp interfaces.[24] $S_{\text{comp}}(q)$ is the structure factor due to the composition fluctuations inside the phase-separated domains.[21] $S_{\text{density}}(q)$ is the scattering structure factor attributed to the density heterogeneities within each phase-separated domain. In particular, the contribution of $S_{\text{density}}(q)$ to $S_t(q)$ cannot be ignored when the SANS measurement is performed at temperatures below or above but close to T_g of the mixture. This is because under this condition, the excess scattering due to the density heterogeneities comes into play.[27] S_{incoh} corresponds to incoherent scattering, which is independent of q. The plateau of the scattering function in the high q limit of the SANS experiment is usually attributed to S_{incoh}.

Since all investigated mixtures, i.e., dPSU/PA and dPSU-R/PA, are highly immiscible, it is conceivable that the composition of the two polymers in each coexisting phase should be close to that of the pure components. Thus, it is assumed that the density heterogeneities present in each domain should be almost identical to those in the corresponding homopolymer samples. Thus, $S_{\text{density}}(q)$ can be approximated by

$$S_{\text{density}}(q) = w_{\text{PA}} S_{\text{density,PA}}(q) + (1 - w_{\text{PA}}) S_{\text{density,PSU}}(q) \quad (6)$$

where $S_{\text{density},i}$ is the structure factor due to the density heterogeneities of the neat ith homopolymer (i = PA or PSU, where PSU = dPSU or dPSU-R) and w_i is the weight fraction of ith homopolymer in the mixture, respectively. Similarly to S_{density}, S_{incoh} is given by

$$S_{\text{incoh}} = w_{\text{PA}} S_{\text{incoh,PA}} + (1 - w_{\text{PA}}) S_{\text{incoh,PSU}} \quad (7)$$

where $S_{\text{incoh},i}$ is the incoherent scattering of neat ith homopolymer. Thus, the structure factor, $S_c(q)$, corrected for the density heterogeneities and incoherent scattering is given by

$$S_c(q) = S_t(q) - S_h(q) = S_{\text{interf}}(q) + S_{\text{comp}}(q) \quad (8)$$

where

$$S_h(q) \equiv S_{\text{density}}(q) + S_{\text{incoh}} \quad (9)$$

Figure 3b shows the scattering structure factor $S_h(q)$ due to the density heterogeneities and the incoherent scattering in the mixtures, where closed circles and open circles correspond to dPSU/PA (50 wt %/50 wt %) and dPSU-R/PA (50 wt %/50 wt %), respectively.

To highlight the significance of the density heterogeneities' contribution to the net scattering structure factor, the scattering profile corrected only for S_{incoh} is compared to the scattering profile corrected for $S_h(q)$. Here, the SANS data from the dPSU/PA mixture (Figure 5) and dPSU-R/PA mixture (Figure 6) after

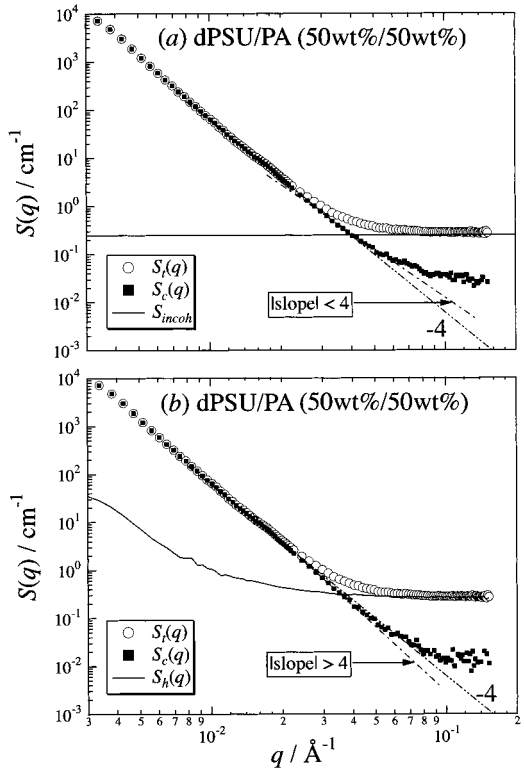

Figure 5. Representative corrections for the SANS analysis using data obtained by annealing for 2 min at 240 °C for the nonreactive system. (a) Comparison between the scattering profile (■) corrected for incoherent scattering (line) and the net scattering profile (○) obtained from dPSU/PA. (b) Comparison between the scattering profile (■) corrected for the density heterogeneities within the phase-separated domains and incoherent scattering (line) and the net scattering profile (○) obtained from dPSU/PA.

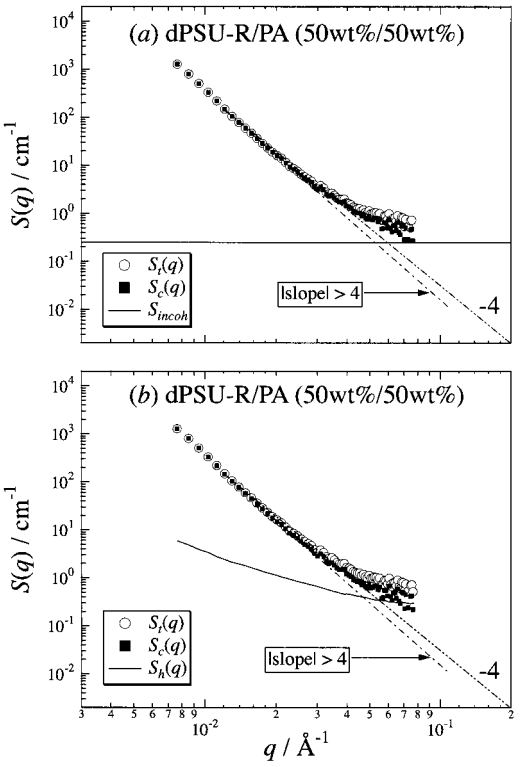

Figure 6. Representative corrections for the SANS analysis using data obtained by annealing for 2 min at 240 °C for the reactive system. (a) Comparison between the scattering profile (■) corrected for incoherent scattering (line) and the net scattering profile (○) obtained from dPSU-R/PA. (b) Comparison between the scattering profile (■) corrected for the density heterogeneities within the phase-separated domains and incoherent scattering (line) and the net scattering profile (○) obtained from dPSU-R/PA.

annealing the sample for 2 min at 240 °C are used. In Figure 5a, S_{incoh} represented by the horizontal solid line is subtracted from the net scattering $S_t(q)$, which is a common data correction scheme for obtaining a structure factor for the case when the contribution of $S_{\text{density}}(q)$ is negligible.[21,25] In Figure 5b, the scattering $S_h(q)$ is subtracted from $S_t(q)$ according to eq 8. Data for the different analysis schemes are shown in parts a and b of Figure 5, where open circles and solid squares represent the uncorrected and corrected profiles, respectively. Comparing these two results after applying different corrections reveals a different q dependence in the range of $q > 0.02$ Å^{-1} [$S(q) \sim q^{-n}$: $n < 4$ in part a and $n > 4$ in part b], indicating that the correction for the density heterogeneities is very important in order to correctly extract interfacial characteristics such as the interfacial width $W_{\text{I,obs}}$, when the interfacial analysis is made on systems where the phase-separated domains are close to or below T_g. Incorrect analyses, ignoring the density heterogeneities, lead to errant interpretations about the interface where the interface is interpreted to have $W_{\text{I,obs}} = 0$ after correction of $S_t(q)$ for $S_{\text{comp}}(q)$ (as will be clarified later in Figure 8a) rather than a nonzero $W_{\text{I,obs}}$.

The same corrections are also performed on the SANS data obtained from the dPSU-R/PA mixture. Namely S_{incoh} is subtracted from $S_t(q)$, in part a of Figure 6, and $S_h(q)$ is subtracted from $S_t(q)$, in part b. The relation $S_c(q) \sim q^{-n}$ with $n > 4$ is obtained in the high q range for both cases shown in parts a and b, in contradiction to the trend observed for dPSU/PA. The difference between the two systems, dPSU/PA and dPSU-R/PA, is primarily attributed to the difference of the intensity level of $S_t(q)$, between the two systems as well as the difference in $W_{\text{I,obs}}$. As for the former, the intensity level of $S_t(q)$ for dPSU-R/PA is much larger than for dPSU/PA, as already described in section III.1. Thus, the correction for S_{incoh} and $S_h(q)$ is less significant for dPSU-R/PA than for dPSU/PA. Even so, the correction for the density heterogeneities is still very important in the dPSU-R/PA system. The interfacial analysis without this correction underestimates the interfacial width as will become clear in the discussion below (see section IV.2). Hence, the SANS intensity distribution $S_c(q)$ corrected for $S_h(q)$ will be used for further analyses and discussions.

The effect of annealing on $S_c(q)$ is shown in Figure 7, where parts a and b correspond to data for the dPSU/PA and the dPSU-R/PA systems, respectively. As a whole, $S_c(q)$'s show the relation $S_c(q) \sim q^{-n}$ with $n \cong 4$ over the range of $q < 0.05$ Å^{-1}, which is mainly attributed to the contribution of the scattering arising from interfaces (Porod's law). The deviation of $S_c(q)$ from the power-law behavior at $q > 0.05$ Å^{-1} is due to the composition fluctuations inside the phase-separated domains.

With respect to the as melt-pressed specimens in the nonreactive blend (dPSU/PA) in part a of Figure 7, the increase of $S_c(q)$ with decreasing q tends to level off at $q < 0.02$ Å^{-1}, where the scattering may be affected by interference between the phase-separated domains. Thus, the entire scattering profile obtained from the as-

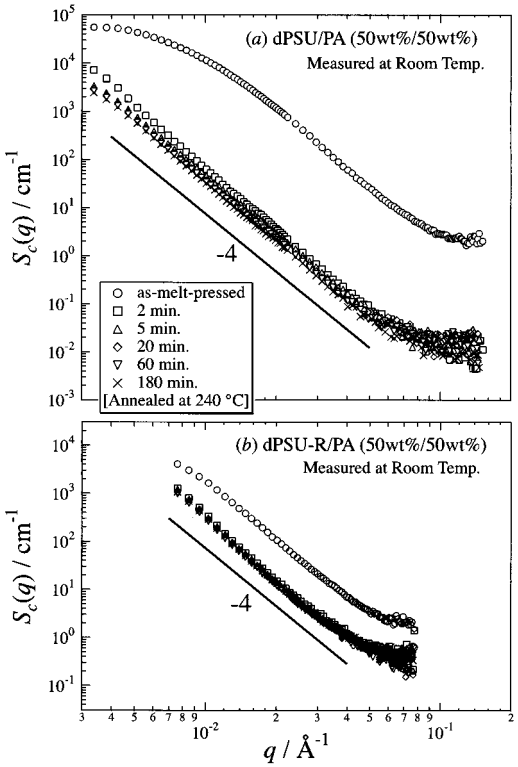

Figure 7. Time-dependent evolution of the SANS profile upon annealing of the as-melt-pressed sample at 240 °C for (a) dPSU/PA and (b) dPSU-R/PA. The data were corrected for the scattering $S_h(q)$ due to the density heterogeneities and incoherent scattering within the phase-separated domains.

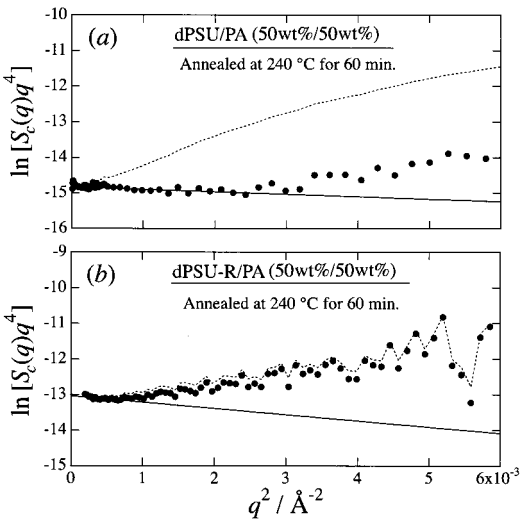

Figure 8. Porod's plots according to eq A4 (●) obtained from the data shown in Figure 7 for 50 wt %/50 wt % (a) dPSU/PA and (b) dPSU-R/PA systems annealed at 240 °C for 60 min and the best-fit straight lines (solid lines) for the respective plots. The dotted lines correspond to the Porod plots for data corrected only for incoherent scattering. The interfacial area density, Σ, and the parameter characterizing the interfacial width, σ, extracted from the plots are (a) $\Sigma = 2.12 \times 10^3$ cm^{-1} and $\sigma = 8.29$ Å and (b) $\Sigma = 1.28 \times 10^4$ cm^{-1} and $\sigma = 13.2$ Å.

melt-pressed sample may be described in terms of random two-phase structures, as proposed by Debye-Büche,[29] with internal composition fluctuations. The drastic decrease in $S_c(q)$ observed in the initial annealing step (2 min at 240 °C) suggests the decrease in the interfacial area density is caused by rapid coarsening of the phase-separated structures. At the same time, part of the scattering curve that shows leveling-off of the intensity with decreasing q may be shifted toward small q and hence be hidden behind the beam stop. After 2 min of annealing, $S_c(q)$ slowly decreases with time, indicating that the phase-separated structures coarsen. The time-dependent change in the interfacial area density will be discussed in section IV.4.

Turning now to part b of Figure 7, the reactive blend, dPSU-R/PA, also exhibits a phase-separated structure that has coarsened drastically in the initial 2 min of annealing at 240 °C, similar to what was observed in the dPSU/PA system. However, $S_c(q)$ does not show any additional change with further annealing, which suggests that pinning inhibits further morphology changes (section IV.4). It is also important to note that the intensity level for the as-melt-pressed specimen is lower for the reactive blend than for the nonreactive blend over the entire q range of $0.007 < q < 0.04$ Å^{-1}.[30] On the other hand, as pointed out in section III.1, after annealing at 240 °C for time periods longer than 2 min the intensity level is higher in dPSU-R/PA than in dPSU/PA. This is interpreted as follows: Upon annealing, the phase-separated domains in the as-melt-pressed samples in dPSU/PA grew to a much larger average size than those in dPSU-R/PA; in other words, the interfacial area density Σ in dPSU/PA is less than in dPSU-R/PA. This important result can be interpreted as pinning of the growth of phase-separated domains in the reactive system due to entropic repulsion between the copolymer brushes formed along the interface.

IV.2. Composition Fluctuations of PSU and PA within the Phase-Separated Domains As Acquired from SANS Data with Bulk Specimens. Figure 8a,b represents $\ln[S_c(q)q^4]$ vs q^2 plots (see section A.1) for the respective bulk mixtures annealed 60 min at 240 °C. In these figures, the filled circles and straight lines represent the experimental data and the best fits based on eq A4, respectively. The interfacial area density Σ is extracted from the intercept at $q^2 = 0$ of the best-fit straight line, and the parameter σ is obtained from the slope (eq A4). The deviation of the data points given by the filled circles from the straight line is due to the $S_{comp}(q)$ contribution to $S_c(q)$. The characteristic parameters σ and Σ obtained for the reactive system were 13 Å and 1.3×10^4 cm^{-1}, respectively, and those for the nonreactive systems were 8.3 Å and 2.1×10^3 cm^{-1}, respectively. The Σ value for the reactive system is larger than the nonreactive system by a factor of 6, reflecting that the domain size of the former is smaller than the latter by the same factor. The corresponding $W_{I,obs}$ ($\sim\sigma$) value for the former is larger than the latter by a factor of 1.6. The two results are consistent and reflect block copolymer formation at the interface, as will be detailed later.

In Figure 8 the dotted lines correspond to Porod's plot for the SANS data corrected only for the incoherent scattering, i.e., $\ln[(S_t(q) - S_{incoh})q^4]$ vs q^2 plot. The comparison between the circles and the dotted lines elucidates the strong contribution of the density heterogeneities to $S_t(q)$, for the mixtures, especially to the data for the dPSU/PA mixture. Thus, it is demonstrated that the interfacial analysis without correcting for the density heterogeneities is meaningless for the dPSU/PA mixture. A significant caveat is that the correction is less important for the dPSU-R/PA mixture than for the dPSU/PA mixture, as shown by a smaller discrepancy between the circles and the dotted line in part b.

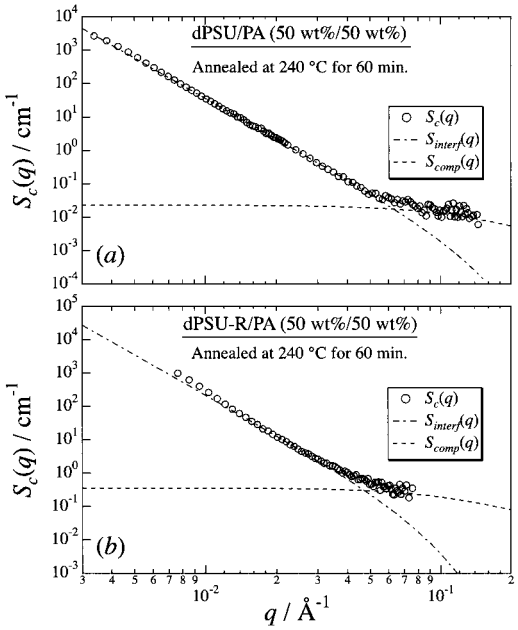

Figure 9. Plots showing that the scattering intensity distributions (open circles) corrected for intraphase heterogeneity and incoherent scattering obtained for 50 wt %/50 wt % (a) dPSU/PA and (b) dPSU-R/PA systems annealed at 240 °C for 60 min. The plots show the importance of two contributions: one due to the scattering arising from the interface (dash−dot lines) and the other due to thermal composition fluctuations inside the phase-separated domains (dashed lines) to the corrected scattering intensity distribution.

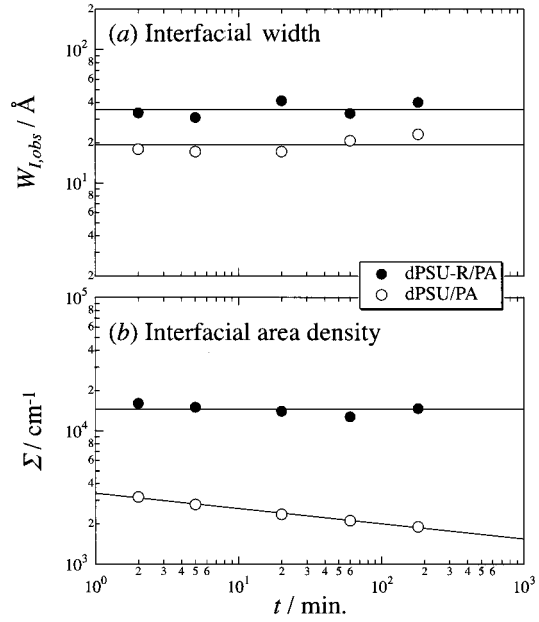

Figure 10. (a) Observed interfacial widths, $W_{I,obs}$, and (b) the interfacial area density, Σ, obtained from the SANS data as a function of annealing time at 240 °C for the dPSU/PA (open symbols) and dPSU-R/PA (filled symbols) systems.

This is simply due to a greater contribution of $S_{interf}(q)$ to $S_t(q)$, relative to that of $S_h(q)$ to $S_t(q)$, in dPSU-R/PA than in dPSU/PA. This in turn is because of a smaller average domain size and hence a larger interfacial area density Σ in the former than in the latter (see eq A1).

According to the Porod plots in Figure 8, $S_c(q)$ can be divided into the two contributions: one due to the interface between the phase-separated domains, $S_{interf}(q)$, and the other to thermal composition fluctuations within them, $S_{comp}(q)$. In Figure 9, the open circles, dash−dot lines, and dashed lines represent $S_c(q)$, $S_{interf}(q)$, and $S_{comp}(q)$, respectively, where the $S_{interf}(q)$ values are the results obtained from eq A1 with the parameters σ and Σ obtained from the Porod's plots in Figure 8. A comparison of Figure 8a,b or Figure 9a,b clearly indicates that the contribution of $S_{comp}(q)$ to $S_c(q)$ is greater in the reactive system than in the nonreactive system. This implies that phase-separated domains in the reactive system contain a greater amount of unlike segments than those in the nonreactive system.

IV.3. Interfacial Width, $W_{I,obs}$, and Interfacial Area Density, Σ, between the PSU and PA Phases As Acquired from SANS Data with Bulk Specimens. The $W_{I,obs}$ values ($=\sqrt{2\pi}\sigma$) and Σ obtained using eqs A2 and A4 together with the plots shown in Figure 8 are themselves plotted as a function of the annealing time at 240 °C in parts a and b of Figure 10, respectively. Values of $W_{I,obs}$ for dPSU-R/PA (filled circles) are larger than values for dPSU/PA (unfilled circles) as seen in part a. Upon annealing at 240 °C, the phthalic anhydride group (R) of dPSU-R and the terminal amino group (NH_2) of PA react at the interface between the dPSU-R phase and the PA phase, forming a block copolymer (dPSU-*b*-PA) in less than 2 min.[20] The block copolymers, once formed, are localized at the interface as a monolayer[20] due to strong segregation forces between the PSU and PA phases, thereby working as a compatibilizer.

As a consequence of block copolymer formation, the interfacial width $W_{I,obs}$ broadens because of the following two factors: (1) The intrinsic interface thickness of block copolymers, $W_{I,diffuse}$, is generally larger than that of the corresponding homopolymer blends, because of an entropic driving force for the chemical junctions of the block copolymer to be in a broader interface.[31,32] (2) The block copolymers formed reduce the interfacial tension,[33] which in turn amplifies the capillary wave fluctuations at the interface between dPSU-R and PA as will be discussed in detail in section IV-4 later. Hereafter, $W_{I,capillary}$ is defined as the interfacial width arising from capillary wave fluctuations.

In addition, as seen in Figure 10b for the dPSU-R/PA system, Σ does not change with time, indicating that the size of the phase-separated domains does not increase after the initial 2 min of the annealing. This is in stark contrast to the phase-separated domains of the dPSU/PA system, which coarsen with time, though very slow, decreasing the interfacial area density that is related to the interfacial free energy. This behavior is in agreement with theoretical predictions for the reactive blending process. The interfacial reaction leads to a rapid buildup of copolymers at the interface until a maximum concentration is reached. A detailed analysis of this phenomenon for the system dPSU//PA was presented previously.[20] The formed diblock copolymers stay localized at the interface and provide a strong barrier against the diffusion of other reactive end group labeled polymers approaching the interface, which de facto stops all further reaction. Additionally, the diblocks also sterically stabilize the phase-separated structure and prevent growth of the domains.[8−11] To quantify the differences between the reactive and nonreactive systems, values of Σ obtained from the analysis through the Porod plots and the characteristic length of the composition fluctuations, Λ_m's, obtained according to section A-3 of the Appendix, are summarized in Table 3.

Table 3. Annealing Time Dependence of the Interfacial Area Density Σ and the Characteristic Domain Size (Average Radius *R* of Droplets or Characteristic Length Λ_m for Bicontinuous Structure)

	dPSU/PA			dPSU-R/PA	
annealing time (min)	$\Sigma \times 10^{-4}$ (cm^{-1})	R (μm)	Λ_m (μm)[a]	$\Sigma \times 10^{-4}$ (cm^{-1})	Λ_m (μm)
0	99.0	0.015	(0.029)	11.0	0.26
2	0.319	4.7	(9.1)	1.60	1.8
5	0.281	5.3	(10)	1.50	1.9
20	0.236	6.4	(12)	1.40	2.1
60	0.212	7.1	(14)	1.28	2.3
180	0.191	7.9	(15)	1.47	2.0

[a] The value in parentheses is the characteristic length Λ_m for the case when the system is assumed to possess a bicontinuous structure.

The domain growth of dPSU-R/PA may have pinned at the time when the interface was effectively saturated by block copolymer formed at the interface. This occurred quite quickly within 2 min after annealing at 240 °C. If additional growth of the domains were to occur, it would require an additional decrease of the interfacial area, which in turn causes stretching of the block copolymers normal to the interface in order to further reduce the interfacial area occupied by a block copolymer chain below its equilibrium value. As stretching the block copolymers increases the free energy, the domain growth can be pinned. Note that this argument assumes the dPSU-R/PA (50 wt %/50 wt %) blend has a bicontinuous spongelike structure[34,35] with a continuous interface in three-dimensional space, rather than a cluster of droplets for one of the components in a matrix of the other component. The dPSU-R/PA data imply that the block copolymers saturate the interface at an early stage of the annealing, hence giving rise to the small value of Λ_m or R (as evaluated from eq A8 or A9 in Appendix A-3) and the large values of Σ (Table 3).

As already pointed out earlier in section IV in conjunction with Figure 2, Σ in the dPSU/PA system is much smaller than that in the dPSU-R/PA system over the time range covered by this study. This indicates that the phase-separated structure in the former system has a much larger size than that in the latter (Table 3). The growth rate of the domain size ($R \sim \Sigma^{-1}$) is very slow, implying that the domains of the nonreactive system will be a cluster of droplets over the observed time scale. We investigated the phase-separated morphology of the system under transmission optical microscopy in order to check the assumption and speculation given above concerning the phase-separated morphology for the reactive and nonreactive systems. Figure 11 shows typical optical micrographs observed for the reactive and nonreactive systems. The micrograph for the reactive system shows a bicontinuous phase-separated structures composed of bright and dark domains with $\Lambda_m \sim 2$ μm, while that for the nonreactive system shows a large bicontinuous structure with $\Lambda_m \sim 100$ μm, each phase of which contains a cluster of droplets composed of the other component polymers with average radius R of $R \sim 10$ μm. These results support the assumption and speculation given above. Thus, in the nonreactive system, the bicontinuous structure keeps growing very rapidly, and its scattering signals degenerate in the small q-window that our SANS apparatus cannot access. The unlike component dissolved initially in each phase may be segregated into droplets which grow very slowly and give rise to the slow decrease of Σ over the time scale of our observation, as shown in Figure 10.

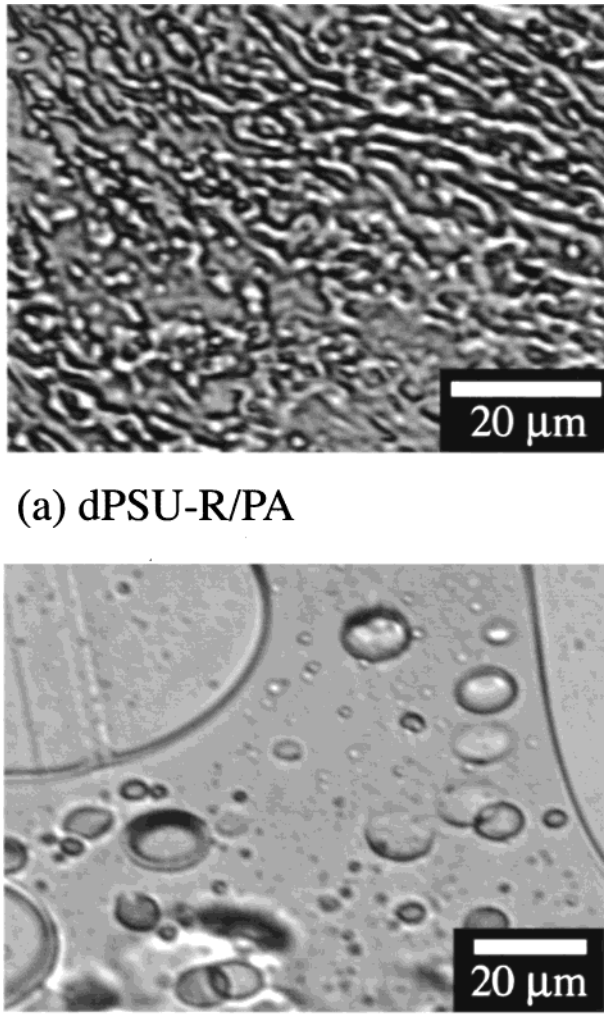

Figure 11. Typical transmission optical micrographs for the dPSU-R/PA (a) and the dPSU/PA (b) specimens, which were annealed at 240 °C for 3 h. The image shown in part a corresponds well with the bicontinuous structure with the characteristic length of the composition fluctuation of $\Lambda_m \sim 2$ μm and that in part b to a cluster structure of droplets having average radius of $R \sim 10$ μm developed inside one of the bicontinuous phases.

IV.4. Interfacial Width, $W_{I,obs}$, between the PSU and PA Layers Obtained from NR. The interfacial widths, $W_{I,obs}$, for the bilayer systems of Si//dPSU//PA// air and Si//dPSU-R//PA//air were determined by fitting the first derivative of the SLD profile with a Gaussian curve[26] whose standard deviation σ is related to the characteristic interfacial width $W_{I,obs}$ by $W_{I,obs} = \sqrt{2\pi}\sigma$.[20] The variation of $W_{I,obs}$ values with annealing time at 210 °C for the reactive and nonreactive bilayer specimens are plotted in Figure 12. The figure also contains two data points corresponding to initial annealing at 210 °C for 755 min and additional annealing at 240 °C for 60 min for each specimen. According to Figure 12, the $W_{I,obs}$ values for the reactive Si//dPSU-R//PA// air system are larger than the values for the nonreactive Si//dPSU//PA//air system. The block copolymers, dPSU-*b*-PA, which were formed at the interface of dPSU-R and PA upon annealing at high temperature, are expected to lower the interfacial tension and hence broaden the interfacial width $W_{I,obs}$ as described in section IV.2.

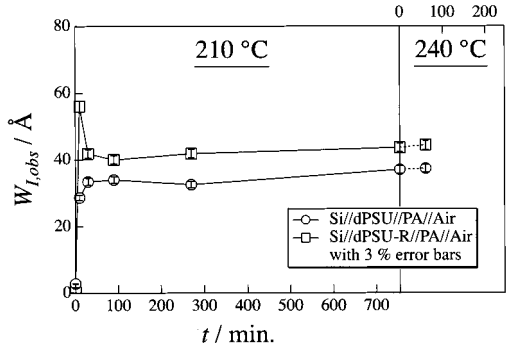

Figure 12. $W_{I,obs}$ values with ±3% error bars for Si//dPSU//PA//air (○) and Si//dPSU-R//PA//air (□) obtained from the fitting analysis for the NR data as a function of annealing time.

Another interesting aspect of Figure 12 is that the data for specimens annealed 30 min at 210 °C show nearly the same value of $W_{I,obs}$ as those annealed for longer times. This indicates that the $W_{I,obs}$ value extracted for specimens annealed more than 30 min at 210 °C and the $W_{I,obs}$ value estimated for the specimen annealed for 60 min at 240 °C have nearly reached the equilibrium values at the respective temperatures. In this sense, it is possible to reasonably discuss the comparison between the data obtained by SANS and those obtained by NR, as will be done in the next section. The anomalous increase of $W_{I,obs}$ observed during the early stages of annealing for the reactive system will be discussed in detail elsewhere.[36]

IV.5. Comparison of $W_{I,obs}$ Values Obtained from SANS and NR for the Reactive and Nonreactive Systems. Figures 13 and 14 provide a comparison between $W_{I,obs}$ values obtained from both NR and SANS data for the nonreactive and reactive systems, respectively. In these figures the filled and open circles correspond to $W_{I,obs}$ values for bilayer (NR) and bulk samples (SANS), respectively. There are two intriguing features found in these figures: (1) $W_{I,obs}$ for the bilayers are larger than those for the bulk mixtures irrespective of the system (reactive and nonreactive systems (Figures 13 and 14)); (2) the difference in values of $W_{I,obs}$ between the bilayer and the bulk mixture for the nonreactive system (Figure 13) is larger than that for the reactive system (Figure 14). For one possible interpretation for these features, the effect of the capillary wave fluctuations at the interface between the PSU and the PA phases on $W_{I,obs}$ needs to be considered. The effect of capillary wave fluctuations on the interfacial width can be approximated by the convolution of a Gaussian distribution of interfacial positions with a step function so that the mean segmental density profile across the interface is given by an error function profile with an interfacial width of $\langle 2\pi(\Delta z)^2\rangle^{1/2}$. Here, $\langle(\Delta z)^2\rangle$ is the mean-square displacement of the interface from its average position due to capillary wave fluctuations. The contributions of the two effects, i.e., the effect associated with the intrinsic interfacial width given by eqs 1 and 2 and the effect of the capillary wave fluctuations to the observed (or net) interfacial width, are assumed to be convoluted. If the two effects are assumed to be given by Gaussian functions with their standard deviations σ_0 and $\langle(\Delta z)^2\rangle^{1/2}$, respectively, it is possible to write the observed interfacial width, $W_{I,obs}$, as

$$W_{I,obs}{}^2 = W_{I,diffuse}{}^2 + W_{I,capillary}{}^2 \qquad (10)$$

where the thickness of the diffuse interface is defined by

$$W_{I,diffuse}{}^2 = 2\pi\sigma_0{}^2 \qquad (11)$$

with σ_0 being the parameter characterizing the diffuse interfacial width, while the width due to the capillary wave fluctuations $W_{I,capillary}$ is defined as

$$W_{I,capillary}{}^2 = 2\pi\langle(\Delta z)^2\rangle \qquad (12)$$

From eqs 12 and A5 one obtains

$$W_{I,capillary} = 2\pi\langle(\Delta z)^2\rangle^{1/2} \sim \gamma^{-1/2}(\ln \lambda_{max})^{1/2} \qquad (13)$$

Since λ_{max}, the maximum wavelength cutoff of capillary waves, for the bilayer of the reactive or nonreactive system is much larger than that for the mixture (see the comparison in the Appendix), the relationship between $W_{I,capillary}$ for the bilayer (defined as $W_{I,cap,bilayer}$) and $W_{I,capillary}$ for the mixture (defined as $W_{I,cap,mixture}$) for a given system at a given temperature is given as

$$\frac{W_{I,cap,mixture}}{W_{I,cap,bilayer}} \sim \left(\frac{\ln \lambda_{max,mixture}}{\ln \lambda_{max,bilayer}}\right)^{1/2} < 1 \qquad (14)$$

which indicates that the contribution of the capillary

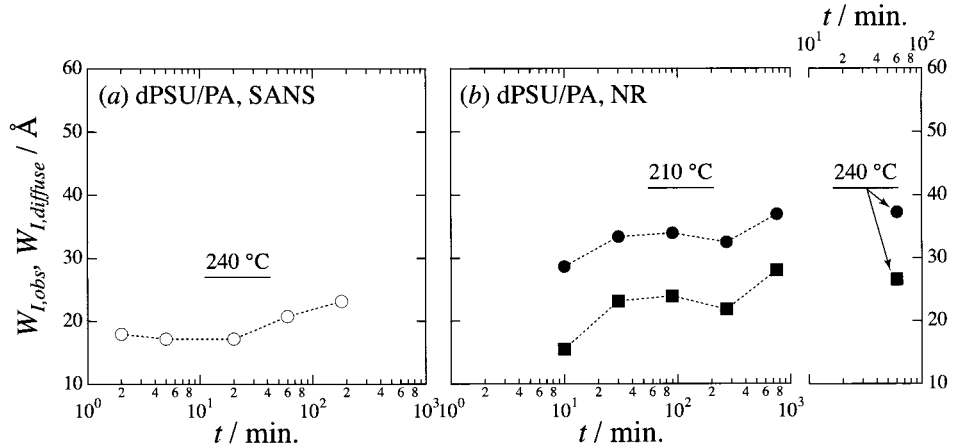

Figure 13. Comparisons of the $W_{I,obs}$ values obtained from the bulk mixtures (○) (a) (dPSU/PA) and those from the bilayers of the nonreactive systems (●) (b) (Si//dPSU//PA//air) at various annealing times at 210 or 240 °C. The filled squares (■) in part b show the $W_{I,diffuse}$ values obtained after correcting for the contribution of capillary wave fluctuations to $W_{I,obs}$.

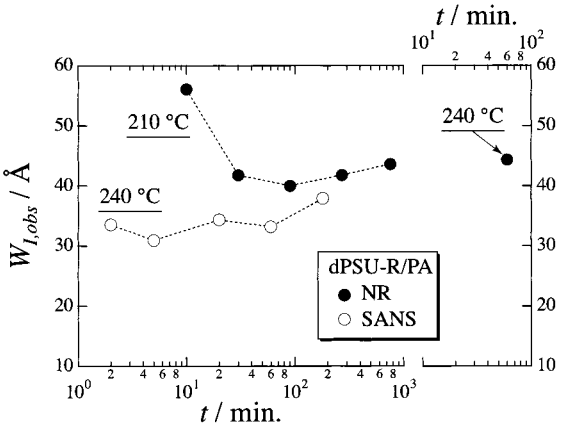

Figure 14. Comparison of $W_{I,obs}$ values obtained from the bilayer (●) and bulk specimens (○) for the reactive system.

wave fluctuations to $W_{I,obs}$ is smaller in the mixture than in the bilayer. Note that $W_{I,cap,mixture}$ values for the mixtures depend on the characteristic length of the phase-separated domains. Since the value $W_{I,diffuse}$ for the mixture and the bilayer should be the same for a given system at a given temperature, eq 14 explains why the observed interfacial width $W_{I,obs}$ in bilayer films is bigger than the bulk system regardless of whether the reactive or nonreactive mixture is studied (feature 1).

According to eqs 12 and A5,

$$W_{I,capillary} \propto \gamma^{-1/2} \tag{15}$$

and according to eqs 2 and A6,

$$W_{I,diffuse} \propto \gamma^{-1} \tag{16}$$

where γ is the interfacial tension. From eqs 15 and 16, the relation

$$W_{I,capillary}/W_{I,diffuse} \propto \gamma^{1/2} \tag{17}$$

is derived for blends. When γ decreases due to an increase of temperature, the left-hand term in eq 17 also decreases, and the contribution of $W_{I,capillary}$ to $W_{I,obs}$ becomes less important than the contribution of $W_{I,diffuse}$. Thus,

$$\left(\frac{W_{I,capillary}}{W_{I,diffuse}}\right)_{higher\ T} < \left(\frac{W_{I,capillary}}{W_{I,diffuse}}\right)_{lower\ T} \tag{18}$$

predicts an intriguing temperature (T) dependence of the relative contributions of $W_{I,capillary}$ and $W_{I,diffuse}$ to $W_{I,obs}$ for blend systems, which deserves future works. Note that eq 16 and hence eq 17 cannot be directly applied to the blend systems with the block copolymer located at interfaces.

For the Si//dPSU//PA//air system, $W_{I,diffuse}$ was estimated from the $W_{I,obs}$ value measured by NR along with the value $\langle(\Delta z)^2\rangle^{1/2}$ calculated according to section A-2 of the Appendix and eqs 10 and 12. The results for $W_{I,diffuse}$ after the correction for $W_{I,capillary}$ are represented by the filled squares in Figure 13b (error bars are smaller than the marker symbols). As seen in Figure 13, the values of $W_{I,diffuse}$ for the bilayer system become almost identical to the bulk mixture $W_{I,obs}$ values, indicating that the contribution of the capillary wave fluctuations to the net interfacial width, $W_{I,obs}$, may be larger in the bilayer system than the bulk mixture. The value $W_{I,diffuse}$ for the nonreactive system (19.4 ± 0.3 Å) is in good agreement with the value theoretically predicted from eq 2 (23.3 Å), as will be detailed in section A-2 of the Appendix. In addition, it is conceivable that the amplitude of capillary wave fluctuations may depend not only on the magnitude of the interfacial tension γ and the lateral extension of the interface λ_{max} but also on shape or curvature of the phase-separated structures, i.e., the mean curvature of the phase-separated structure. Such a possibility provides a plausible reason why the capillary wave fluctuations contribute less significantly to $W_{I,obs}$ in the bulk polymer mixture than in the bilayer film.

Unfortunately, no data concerning the interfacial tension between dPSU-R and PA exists (note that the interfacial tension between PSU and PA is given in section A-2 in the Appendix). Nonetheless, it is conceivable that the interfacial tension of the reactive system may be comparatively lower than the nonreactive system due to compatibilization through dPSU-*b*-PA block copolymer formation. This factor would make the values of $W_{I,obs}$ for the reactive system larger than the nonreactive system as seen by comparing the results shown in Figures 13 and 14 primarily because this would make the value $W_{I,capillary}$ for the reactive system larger than the nonreactive system. Additionally, further changes in the relative contribution of $W_{I,capillary}$ and $W_{I,diffuse}$ to $W_{I,obs}$ would contribute to feature 2 described above.

V. Conclusion

The interfacial width of a nonreactive system (dPSU and PA) and a reactive system (dPSU-R and PA blends, where dPSU-R can react with PA to form dPSU-*b*-PA block copolymer) were measured by SANS (bulk mixtures) and NR (bilayer films) for a series of quench experiments as a function of annealing time. The analysis of the SANS data revealed that two kinds of corrections resulting from heterogeneities within phase-separated domains need to be taken into account during a Porod plot analysis: One is the scattering contribution of density heterogeneities arising during vitrification and a second scattering contribution caused by local composition fluctuations frozen inside the phase-separated domains. The NR data were corrected for the heterogeneities by subtracting the background measured by off-specular reflectivity from the measured specular reflectivity.The corrected data were analyzed using a standard multilayer fitting method for modeling the scattering length density profiles. Taking the contribution of capillary wave fluctuations into account, which were shown to be more significant for NR than for SANS, the intrinsic interfacial width for the nonreactive system can be evaluated for bulk (SANS) as well as bilayer (NR) systems. This intrinsic interfacial width for the annealed specimens of the nonreactive bulk mixtures derived from SANS measurements is comparable within experimental error to the value obtained from NR measurements on bilayer films. The relative contribution of the capillary wave fluctuations to the observed interfacial width $W_{I,obs}$ was found to be smaller for the reactive than the nonreactive system.

The major changes in the interfacial width as well as the interfacial area density occurred very quickly (less than 2 min) upon annealing in all experiments. The interfacial widths observed in the reactive system by SANS and NR are both larger than the nonreactive

system. This is interpreted as a consequence of dPSU-*b*-PA diblock copolymer formation at the interface between the dPSU-R and PA phases and the entropic driving for their chemical junctions to be in a broader interface. The time dependence of the scattering reveals that dPSU-*b*-PA copolymer formation also arrests coarsening of the phase-separated structures in the reactive system, which is probably due to steric hindrance of the domain growth by the block copolymers at the interface. Without diblocks, the phase-separated structure in the nonreactive system grew with time and become substantially larger than that in the reactive system, thereby reducing the total interfacial area and the free energy of the system. This observation is in good agreement with theoretical predictions for reactive blending processes.[8−11]

Acknowledgment. T.H. and M.W. gratefully acknowledge the German Ministry for Science (BMBF Project 03N30283) for financial support of this work. H.G. thanks the Alexander von Humboldt Foundation for financial support. We also acknowledge Mr. Kazuhiro Yamauchi for his experimental support.

Appendix

A.1. General Features of Scattering from Interfaces between Phase-Separated Domains. In general, the q range over which the scattering intensity distribution reflects the interface between phase-separated domains is known as the Porod region. In this q range[24]

$$S_c(q,t) = 2\pi\Delta\rho^2\Sigma(t)q^{-4}\exp[-\sigma(t)^2q^2] \qquad \text{(A1)}$$

Here, $\sigma(t)$ is a time-dependent parameter characterizing the interfacial width and $\Sigma(t)$ is the interfacial area density (the interfacial area per unit volume). Additionally, $\sigma(t)$ is related to the observed (or net) interfacial width $W_{\mathrm{I,obs}}$ by

$$W_{\mathrm{I,obs}} = \sqrt{2\pi}\sigma \qquad \text{(A2)}$$

The contrast factor, $\Delta\rho^2$, is related to the composition difference between the two coexisting phases by

$$\Delta\rho^2 = [(b_1/V_1) - (b_2/V_2)]^2 \qquad \text{(A3)}$$

where b_i and V_i correspond to the scattering length of component i per monomer unit and monomer volume, respectively.

From eq A1, one obtains

$$\ln[S_c(q,t)q^4] = \ln[2\pi\Delta\rho^2\Sigma(t)] - \sigma(t)^2q^2 \qquad \text{(A4)}$$

which shows that $\ln[S_c(q,t)q^4]$ at a fixed t plotted against q^2 follows a straight line, and the parameters $\Sigma(t)$ and $\sigma(t)$ can be extracted from the intercept at $q^2 = 0$ and the slope of the straight line using $\Delta\rho^2 = 2.72 \times 10^5$ cm^{-2} for the mixture of dPSU (or dPSU-R) and PA. Note that a detailed discussion regarding the interfacial analysis is available elsewhere.[37]

A.2. Calculation of the Amplitude of the Capillary Wave Fluctuations between PSU and PA. The theory of capillary wave fluctuations was developed primarily for a liquid/vapor interface.[38,39] Extension of these ideas to polymeric systems is straightforward. The basic results of these treatments are an expression for $\langle(\Delta z)^2\rangle$, the mean-squared displacement of the interface from its average position:[16]

$$\langle(\Delta z)^2\rangle = \frac{k_{\mathrm{B}}T}{2\pi\gamma}\ln\left(\frac{\lambda_{\max}}{\lambda_{\min}}\right) \qquad \text{(A5)}$$

where γ is the interfacial tension between two immiscible homopolymers A and B, and $\lambda_{\min}$ and $\lambda_{\max}$ are the minimum and maximum wavelengths of the capillary wave fluctuations. The long wavelength cutoff $\lambda_{\max}$ is proportional to the lateral extension of the interface.

The lateral extension of the interface for the bilayer is quite large compared to bulk phase-separated domain structures. However, $\lambda_{\max}$ in bilayer films is limited by the lateral coherence length for NR measurements which generally depend on q. We estimated that the coherence length increases to values as large as 150 μm by lowering q down to $q \cong 0.012$ Å^{-1}. In bulk phase-separated structures $\lambda_{\max}$ will be on the order of the inverse of the interfacial curvature of the domains, which will be less than 0.015−7.9 μm for dPSU/PA and 0.26−2.3 μm for dPSU-R/PA (see Table 3). The large interfacial curvatures in the phase-separated domain structures make $\lambda_{\max}$ small compared to the bilayer system possessing nearly zero mean curvature. The intrinsic interfacial width is expected to provide a good estimate of $\lambda_{\min}$,[40] which might be 20−30 Å. The interfacial tension can be calculated from the expression given by[12,18]

$$\gamma = l\rho_0 k_{\mathrm{B}}T\sqrt{\chi/6} \qquad \text{(A6)}$$

where l is an average of the statistical segment lengths for the two homopolymers, which is simply their arithmetic mean for a small relative difference between the two segment lengths. For simplicity, the two homopolymers are assumed to have equal segment lengths. According to work regarding the miscibility of a dPSU and hydrogenous PSU-R mixture reported by Takeno et al.,[28] one obtains $l = 27$ Å. The volume occupied by one PSU repeat unit is $1/\rho_0 = 648$ Å^3. The interfacial tensions between PSU and PA homopolymers measured at 280 and 300 °C by the spinning drop method are 9.1 ± 0.7 and 7.5 ± 0.6 mN/m, respectively.[41] As it is not possible to measure the interfacial tension at lower temperatures (i.e., 210 and 240 °C), because of the high viscosity of PSU and PA, the Flory−Huggins segmental interaction parameter χ[13] was calculated for $T = 280$ and 300 °C using eq A6. By assuming a linear temperature dependence, $\chi(T)$ can be estimated as

$$\chi(T) = -4.70 + 2.87 \times 10^3/T \qquad \text{(A7)}$$

By extrapolating to $T = 240$ °C, χ can be calculated from eq A7 and γ can be estimated as $\gamma = 11.4$ mN/m from eq A6 using the aforementioned values for l, ρ_0, and so on. Subsequently, substitution of this value for γ into eq A5, with $1.5 \times 10^6/30 \le \lambda_{\max}/\lambda_{\min} \le 1.5 \times 10^6/20$, gives $\langle(\Delta z)^2\rangle^{1/2} = 10.4 \pm 0.1$ Å and $W_{\mathrm{I,capillary}} = 26.1 \pm 0.3$ Å for the bilayer film of the nonreactive system. Equation 10 together with $W_{\mathrm{I,obs}} = 37.3$ Å and $W_{\mathrm{I,capillary}} = 26.1 \pm 0.3$ Å yields $W_{\mathrm{I,diffuse}} = 26.6 \pm 0.3$ Å for the bilayer. Thus, $W_{\mathrm{I,diffuse}}$ is approximately equal to $W_{\mathrm{I,capillary}}$ in this case. The value of $W_{\mathrm{I,diffuse}}$ obtained at 240 °C (26.6 ± 0.3 Å) is consistent with the theoretical value 23.3 Å calculated from eq 2. We did not evaluate $W_{\mathrm{I,capillary}}$ for the bulk mixture, simply because we do not know how to evaluate

λ_{max} for the phase-separated system for the bulk system at this moment. The evaluation will be left to future work.

A.3. Characteristic Length Λ_m Acquired from SANS. According to Koga et al.,[42] the relation

$$\Sigma = 2\pi \times 0.46/\Lambda_m \quad \text{(A8)}$$

holds between the interfacial area density Σ and the characteristic length of the composition fluctuations Λ_m for the case of bicontinuous phase-separated structures. If a phase-separated structure contains a cluster of spherical droplets of an average radius R, the following relationship is obtained between R and Σ

$$R = 3\phi_{sphere}/\Sigma \quad \text{(A9)}$$

where ϕ_{sphere} is volume fraction of the droplets in the system. The values Λ_m and R calculated from Σ are listed in Table 3.

References and Notes

(1) Feng, Y.; Weiss, R. A.; Karim, A.; Han, C. C.; Keiser, H.; Peiffer, G. *Macromolecules* **1996**, *29*, 3918.
(2) Koriyama, H.; Oyama, H. T.; Ougizawa, T.; Inoue, T.; Weber, M.; Koch, E. *Polymer* **1999**, *40*, 6381.
(3) Triacca, V. J.; Ziaee, S.; Barlow, J. W.; Keskkula, H.; Paul, D. R. *Polymer* **1991**, *32*, 1401.
(4) Scott, C.; Macosko, C. *J. Polym. Sci., Part B: Polym. Phys.* **1994**, *32*, 205.
(5) Jiao, J. B.; Kramer, E. J.; de Vos, S. D.; Möller, M.; Koning, C. *Macromolecules* **1999**, *32*, 6261.
(6) Jiao, J. B.; Kramer, E. J.; de Vos, S. D.; Möller, M.; Koning, C. *Polymer* **1999**, *40*, 3585.
(7) Kressler, J.; Mülhapt, R.; Weber, M. *J. Appl. Polym. Sci.* **1997**, *65*, 567.
(8) Fredrickson, G. H.; Milner, S. T. *Macromolecules* **1996**, *29*, 7386.
(9) Fredrickson, G. H. *Phys. Rev. Lett.* **1996**, *76*, 3440.
(10) OShaughnessy, B.; Sawhney, U. *Macromolecules* **1996**, *29*, 7230.
(11) OShaughnessy, B.; Sawhney, U. *Phys. Rev. Lett.* **1996**, *76*, 3444.
(12) Helfand, E.; Tagami, Y. *J. Chem. Phys.* **1972**, *56*, 3592.
(13) Flory, P. J. In *Principles of Polymer Chemistry*; Cornell University Press: Ithaca, NY, 1971.
(14) Fernandez, M. L.; Higgins, J. S.; Penfold, J.; Ward, R. C.; Shackleton, C.; Walsh, D. J. *Polymer* **1988**, *29*, 1923.
(15) Anastasiadis, S. H.; Russell, T. P.; Satija, S. K.; Majkrzak, C. F. *J. Chem. Phys.* **1990**, *92*, 5677.
(16) Shull, K. R.; Mayes, A. M.; Russell, T. P. *Macromolecules* **1993**, *26*, 3929.
(17) Edwards, S. *Proc. Phys. Soc. London* **1965**, *85*, 613.
(18) Helfand, E.; Sapse, A. M. *J. Chem. Phys.* **1975**, *62*, 1327.
(19) Kerle, T.; Klein, J.; Binder, K. *Phys. Rev. Lett.* **1996**, *77*, 1318.
(20) Hayashi, M.; Grüll, H.; Esker, A.; Weber, M.; Sung, L.; Satija, S. K.; Han, C. C.; Hashimoto, T. *Macromolecules* **2000**, *17*, 641.
(21) Hashimoto, T.; Jinnai, H.; Hasegawa, H.; Han, C. C. *Physica* **1994**, *A204*, 261.
(22) Darwin, C. G. *Philos. Mag.* **1914**, *27*, 315, 675. Ewald, P. P. *Ann. Phys.* **1917**, *49*, 1, 117; *54*, 519; *Z. Kristallogr.* **1937**, *97*, 1. Von Laue, M. *Ergeb. Exakt. Naturwiss.* **1931**, *10*, 133. Regarding the principle of reflectivity, see for example: Parratt, L. G. *Phys. Rev.* **1954**, *95*, 359.
(23) Born, M. *Z. Phys.* **1926**, *37*, 863; *38*, 803.
(24) Porod, G. *Kolloid Z.* **1951**, *124*, 83; **1952**, *125*, 51.
(25) Hasegawa, H.; Sakrai, S.; Takenaka, M.; Hashimoto, T.; Han, C. C. *Macromolecules* **1991**, *24*, 1813.
(26) Welp, K. A.; Co, C. C.; Wool, R. P. *J. Neutron Res.* **1999**, *8*, 37.
(27) Fischer, E. W. *Physica* **1993**, *A201*, 183.
(28) Takeno, H.; Hashimoto, T.; Weber, M.; Schuch, H.; Koizumi, S. *Polymer* **2000**, *41*, 1309.
(29) Debye, P.; Bueche, A. M. *J. Appl. Phys.* **1949**, *20*, 518.
(30) This may be a consequence of the fact that the molecular weight of dPSU-R is larger than that of dPSU. This fact in turn causes a larger segregation power in dPSU-R/PA than in dPSU/PA, and as a consequence the phase-separated domains may grow to a larger average size during the sample preparation process in the system dPSU-R/PA compared to the dPSU/PA system.
(31) Helfand, E. *Macromolecules* **1975**, *8*, 552. Helfand. E.; Wasserman, Z. R. *Macromolecules* **1976**, *9*, 879.
(32) The same physics may be applied to account for the difference in the interface thickness between the blends with and without the block copolymer brushes formed in the reactive system.
(33) Leibler, L. *Macromol. Chem., Macromol. Symp.* **1988**, *16*, 1.
(34) Hashimoto, T.; Jinnai, H.; Nishikawa, T.; Koga, T.; Takenaka, M. *Prog. Colloid Polym. Sci.* **1997**, *106*, 118.
(35) Hashimoto, T.; Koga, T.; Jinnai, H.; Nishikawa, Y. *Nuovo Cimento* **1998**, *20*, 1947.
(36) Hayashi, M.; Hashimoto, T.; Weber, M.; Grüll, H.; Esker, A. R.; Han, C. C.; Satija, S. K., to be submitted.
(37) Hashimoto, T.; Takenaka, M.; Jinnai, H. *J. Appl. Crystallogr.* **1991**, *24*, 457.
(38) Buff, F. P.; Lowett, R. A.; Stilinger, F. H. *Phys. Rev. Lett.* **1965**, *15*, 621.
(39) Rowlinson, J.; Widom, B. In *Molecular Theory of Capillary*; Oxford University Press Inc.: New York, 1982.
(40) Sterrazza, M.; Xiao, C.; Jones, R. A. L.; Bucknall, D. G.; Webster, J.; Penfold, J. *Phys. Rev. Lett.* **1997**, *78*, 3693.
(41) Schoolenberg, G. E.; During, F.; Ingenbleek, G. *Polymer* **1998**, *39*, 765.
(42) Koga, T.; Kawasaki, K.; Takenaka, M.; Hashimoto, T. *Physica* **1993**, *A198*, 473.

MA000661G